Since January 2020 Elsevier has created a COVID-19 resource centre with free information in English and Mandarin on the novel coronavirus COVID-19. The COVID-19 resource centre is hosted on Elsevier Connect, the company's public news and information website.

Journal of Photochemistry & Photobiology, B: Biology 235 (2022) 112551

Contents lists available at ScienceDirect

Journal of Photochemistry & Photobiology, B: Biology

journal homepage: www.elsevier.com/locate/jphotobiol

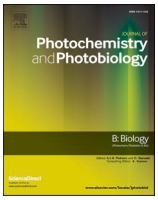

Flexible, disposable photocatalytic plastic films for the destruction of viruses

Ri Han [a,1], Jonathon D. Coey [b,1], Christopher O'Rourke [a], Connor G.G. Bamford [b], Andrew Mills [a,*]

[a] School of Chemistry and Chemical Engineering, Queens University Belfast, Stranmillis Road, Belfast BT9 5AG, UK
[b] Wellcome-Wolfson Institute for Experimental Medicine (WWIEM), Queens University Belfast, School of Medicine, Dentistry and Biomedical Sciences, 96 Lisburn Road, Belfast BT9 7BL, UK.

ARTICLE INFO

Keywords:
Photocatalysis
Titanium dioxide
Viruses
SARS
Cool white light

ABSTRACT

A thin, 30 μm, flexible, robust low-density polyethylene, LDPE, film, loaded with 30 wt% P25 TiO_2, is extruded and subsequently rendered highly active photocatalytically by exposing it to UVA (352 nm, 1.5 mW cm^{-2}) for 144 h. The film was tested for anti-viral activity using four different viruses, namely, two strains of Influenza A Virus (IAV), WSN, and a recombinant PR8, encephalomyocarditis virus (EMCV), and SARS-CoV-2 (SARS2). The film was irradiated with either UVA radiation (352 nm, 1.5 mW cm^{-2}; although only 0.25 mW cm^{-2} for SARS2) or with light from a cool white fluorescent lamp (UVA irradiance: 365 nm, 0.047 mW cm^{-2}). In all cases the films exhibited an average virus inactivation rate of >1.5log/h. In the case of SARS2, the rates were > 2log/h, with the rate determined using a dedicated, low intensity UVA source (0.25 mW cm^{-2}) only 1.3 x's faster than that for a cool white lamp (UVA irradiance = 0.047 mW cm^{-2}), which suggests that SARS2 is particularly prone to photocatalytic inactivation even under low UV irradiation conditions, such as found in a room lit with just white fluorescent tubes. This is the first example of a flexible, very thin, photocatalytic plastic film, produced by a scalable process (extrusion), for virus inactivation. The potential of such a film for use as a disposable, self-sterilising thin plastic material alternative to the common, non-photocatalytic, inert equivalent used currently for curtains, aprons and table coverings in healthcare is discussed briefly.

1. Introduction

There are over 200 viruses that can cause disease in humans, including, influenzas A and B (IAV and IBV, respectively), severe acute respiratory syndrome coronavirus 2 (SARS-CoV-2), varicella-zoster virus (chickenpox) and the measles virus. Respiratory-borne viruses, which remain major clinical problems, are spread by coughing, sneezing or talking, all of which produces small (< 5 μm) water droplets containing infectious virus particles that are able to travel many meters distance and are readily inhaled. These droplets also fall on surfaces (fomites) such as plastics, metals or fabrics, which facilitate the subsequent transmission of these and other infectious virus particles, usually via hand to face contact. It is now generally accepted that fomites play a key role in the spread of viruses in a wide range of environments, including hospitals, nursing homes, schools and offices [1–3].

Although viruses do not multiply outside of the host cells [4], many, including SARS-CoV-2, can survive several days on fomites [5], and this feature can contribute markedly to their transmissibility. Thus, surface disinfection, using bleach or alcohol, is commonly employed to prevent the fomite-based transmission of microbial infectious species, such as viruses. More recently, there is a growing interest in self-sterilising surfaces, such as ones with a photocatalytic coating [6].

The semiconductor photocatalyst that is used in all commercial photocatalytic products, such as self-cleaning glass [7], plastics [8], fabrics [9], tiles [10] and paints [11], is titanium dioxide, TiO_2. Its popularity lies in the fact that it is inexpensive, chemically inert, biologically non-toxic and very effective as a photocatalyst; not surprisingly, there have been many reports of its use in the photocatalysed destruction of viruses, such as the influenza A [12], herpes simplex [13], norovirus [14], hepatitis B [15] and the SARS-CoV-2 viruses [16–19].

The major infectious entity of a virus exists in the form of independent particles, or virions, consisting of, (i) the genetic material, i.e. the

* Corresponding author.
E-mail address: andrew.mills@qub.ac.uk (A. Mills).
[1] Contributed equally to this work.

https://doi.org/10.1016/j.jphotobiol.2022.112551
Received 8 May 2022; Received in revised form 26 July 2022; Accepted 21 August 2022
Available online 25 August 2022

DNA or RNA that encodes structural and non-structural proteins required for replication, (ii) a protein shell, the capsid, which surrounds and protects the genetic material and, in some cases, (iii) an outer envelope of lipids, which incorporates membrane-bound glycoproteins that are responsible for virion entry into the target host cells. In the photocatalysed destruction of a virus, the photocatalyst produces reactive oxygen species, ROS, such as OH radicals, $OH^{\bullet}$, superoxide radicals, $O_2^{-\bullet}$ and $HO_2^{\bullet}$, and hydrogen peroxide, H_2O_2, which are able to effect the peroxidation of the virus's lipid membrane, carbonylation of its proteins, and degradation of its genetic material, thereby destroying the virus [6,20].

In photocatalysis, the above ROS's are generated via *ultra*-bandgap irradiation of TiO_2, which produces holes in the valence band, h^+, that are able to oxidise adsorbed OH^- groups to $OH^{\bullet}$ and conductance band electrons, e^-, that are able to reduce adsorbed O_2 to $O_2^{-\bullet}$ and $HO_2^{\bullet}$, which in turn can be reduced further to H_2O_2, which itself can act as a potential source of $OH^{\bullet}$. The various ROS-generating photocatalytic processes associated with the UV irradiation of TiO_2 particles, in film or powder form, are summarised in the schematic illustration in Fig. 1.

A clear limitation regarding the use of TiO_2-based photocatalytic films as self-sterilising surfaces is the fact that they only absorb UV radiation, which would appear to suggest that they would be inappropriate for use indoors. However, the most popular form of indoor fluorescent white lighting, a cool white lamp, actually emits some UV, at 365 and 313 nm, due to the electronically excited mercury vapour contained within, as illustrated in Fig. 2.

In addition, ca. 4–5% of the energy of the solar spectrum falls in the UV, so that on a bright summer's day the UV irradiance is ca. 4.5 mW cm^{-2} [21], and, after passing through 3 mm thick window glass, the UV solar spectrum is still significant, i.e. typically, 3.7 mW cm^{-2} for a bright summer's day, as illustrated in Fig. 2. Thus, it is perhaps not too surprising that several groups have shown that TiO_2 films are effective as self-sterilising surfaces even under indoor lighting or room daylight conditions [14,15,17].

In practice, a more significant barrier to the widespread use of self-sterilising photocatalytic films is posed by the need for both physical robustness *and* high activity, which is not easily achieved in practice. For example, most commercial photocatalytic films, such as on glass and tiles, are very robust, but not particularly active, although sufficiently active to fulfil their intended role, namely, to utilise the ambient solar UV to destroy the small level (ca. 20 nm per h) of organic pollutants that adsorb on a typical, usually exterior, surface, such as glass [22,23]. Not surprisingly, such photocatalytic materials lack the activity to be self-sterilising, especially under indoor illumination conditions, where robustness *and* high activity are essential. As a consequence, such materials are usually promoted as 'self-cleaning', but not self-sterilising.

In contrast, in many of the research studies of self-sterilising photocatalytic films, the latter are highly active but not particularly robust. For example, many are produced using an aqueous dispersion of an active photocatalytic powder, such as P25 TiO_2, to coat the supporting substrate, usually glass or ceramic, but rely on the weak van der Waals forces produced by drying the coating in air at room temperature to fix the photocatalyst powder particles [17,19,24]. In some cases, more robust photocatalytic films are produced by employing a high temperature, annealing step, typically 450 °C for 1 h [14,16,25,26], but this, obviously, then restricts the choice of supporting substrate to ones that are stable at such high temperatures, such as glass or tiles, and which are not flexible.

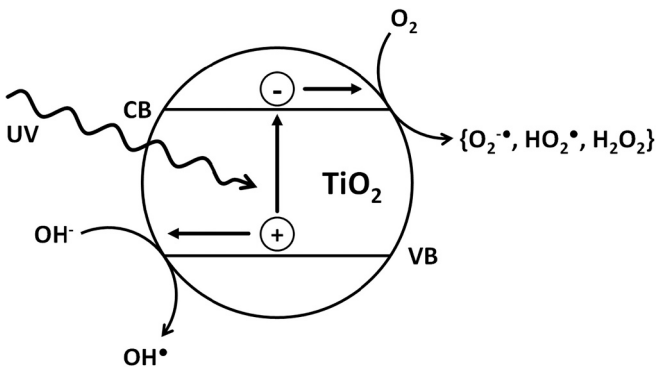

Fig. 1. Schematic illustration of the generation of ROS on the surface of a TiO_2 photocatalytic particle, upon its irradiation with UV radiation.

Disposable, highly flexible plastic films, such as aprons, tablecloths and curtains, are commonly used to help reduce the transmission of disease, and it follows that the efficacy of these materials in the latter role would be enhanced significantly if they could be made self-sterilising. As noted above, in theory at least, one way this might be achieved is by coating the plastic with a flexible, robust and active photocatalytic film. Such a flexible composite material is likely to be particularly interesting if it could be made at no great additional cost compared to the uncoated, original disposable plastic material. However, although some self-sterilising work has been conducted on plastic substrates, the photocatalytic films usually comprise a loose coating of photocatalyst powder on the plastic [18,27], which renders them active but *neither* robust, or flexible. Encouragingly, Lam and his *co*-workers have used a solvent casting technique to produce films of polyethylene, polystyrene and LDPE impregnated with ZnO-based photocatalysts which exhibit antibacterial activity, although the method of production doesn't appear appropriate for the scalable production of very thin and flexible films [28,29].

Thus, in this paper we describe the scalable production, characterisation and testing of a flexible plastic film, the production of which is easily scaled, with a *robust* and very *active* photocatalytic coating, that is able to effect the destruction of a range of different viruses, including SARS-CoV-2, under simulated, window glass filtered, solar UV irradiation and room light conditions. To our knowledge this is the first example of a flexible, very thin, photocatalytic plastic film, produced by a scalable process (extrusion), for virus inactivation.

2. Experimental

2.1. Materials

The photocatalytic plastic films were produced using low density polyethylene, LDPE, powder (Ultrapolymers Warrington, UK) and P25 TiO_2 nanoparticles (Evonik Industries, Essen, Germany). All other chemicals were obtained from Merck Life Science UK Ltd. (Gillingham, UK) and used as received. All aqueous solutions were made using doubly distilled, de-ionised water.

Four viruses were used in this work, namely, (i) two strains of Influenza A Virus (IAV), namely, WSN, and a recombinant PR8 (original sample provided by Prof. Yoshihiro Kawaoka, University Wisconsin, [30]) which expressed the red fluorescent protein mCherry, (ii) encephalomyocarditis virus (EMCV), and (iii) SARS-CoV-2 (passage 2 D614G/B.1.177/"BT20.5″ strain, original sample provided by Dr. Deirdre Gilpin, Queens University Belfast). Briefly, (i) two strains of Influenza A Virus (WSN and PR8) were chosen as IAV is a prototypic enveloped virus and relevant as a virus that causes pandemics and epidemics in humans, (ii) EMCV was chosen as a prototypic non-enveloped virus to investigate the activity of TiO_2 against a virus predicted to have greater surface stability than IAV and (iii) SARS-CoV-2 was chosen due to its relevance as a pandemic virus.

IAV (PR8/WSN) and SARS-CoV-2 virions, henceforth referred to as 'SARS2', comprise roughly spherical particles of ca. 100 nm in diameter with a phospholipid bilayer outer envelope, with (glyco)proteins 'spikes' embedded within it [31–33]. The latter are essential for infectivity, as they allow the virus particles to bind and enter the host cell. Inside the envelope is an additional shell of matrix protein, the capsid, inside of which lies the viral genome of about 15–30 kb (RNA) closely

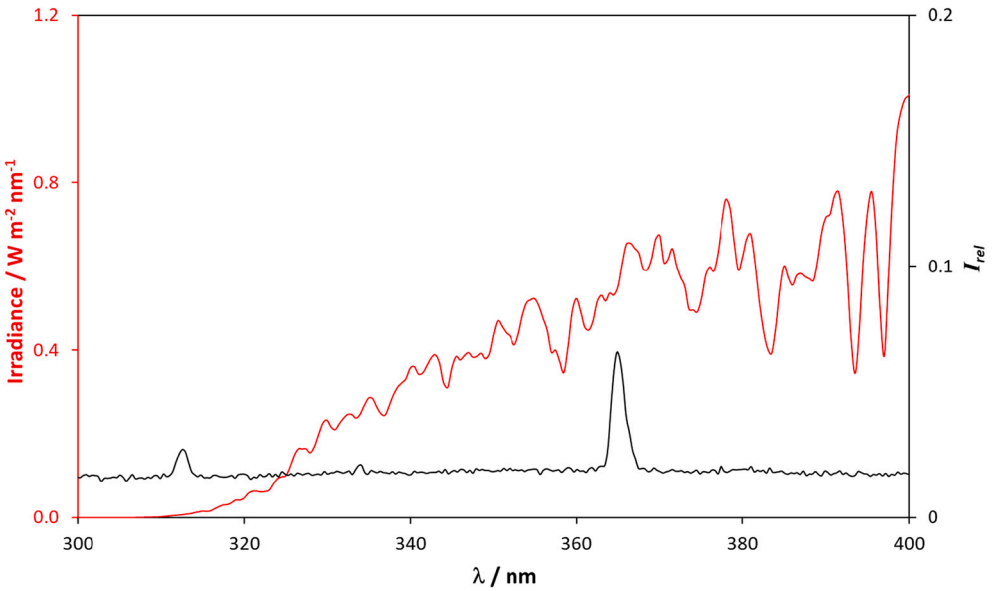

Fig. 2. Emission spectra of the sun (after passing through 3 mm window glass; red line and axis) and a cool white fluorescent lamp (two 15 W tubes, at a distance of 35 cm; black line and y-axis). The measured total UV irradiances for these two light sources are 3.7 and 0.047 mW cm^{-2}, respectively. (For interpretation of the references to colour in this figure legend, the reader is referred to the web version of this article).

associated with N protein (nucleoprotein). IAV and SARS2 cause mainly respiratory disease in people, infecting cells in the nose, throat, respiratory tract, and lungs [33]. IAV is a global endemic virus which routine vaccination helps control, although seasonal epidemics occur annually. SARS2 is best characterised still as a pandemic virus but it is likely to become, like IAV, a global endemic species over the next few years.

EMCV virions are icosahedral, non-enveloped, particles of ca. 30 nm in diameter, comprising a capsid, on the surface of which are areas that bind to the cell and facilitate uptake inside the host cell [31,34]. Inside the capsid is a genome of about 8 kb (RNA). EMCV is a cardiovirus and although it does not cause disease in people, it does in other animals, such as pigs and certain non-human primates, and there are human pathogenic cardioviruses [34]. EMCV is spread via ingestion and, as it is non-enveloped, is very stable. EMCV has been included in this study as an example of an easy-to-work-with, non-enveloped virus, but more well-known human pathogenic, non-enveloped, viruses include, adenovirus, rotavirus and norovirus.

Virus stocks were prepared and titrated in cell culture using standard techniques and the following host cells, (i) Madin-Darby canine kidney, i.e. MDCK, cells for IAV, (ii) Vero cells for EMCV, and (iii) VAT cells, i.e. VeroE6 cells expressing human ACE2 and TMPRSS2, for SARS2 [35,36]. Dulbecco's modified Eagle's Medium (DMEM) with 10% *v*/v Foetal calf serum (FCS) with penicillin and streptomycin (1% *v*/*v*), was used for all routine cell and virus cultures, except FCS was omitted for work with PR8 and replaced instead with 0.3 wt% bovine serum albumin (BSA) and TPCK (L-1-tosylamido-2-phenylethyl chloromethyl ketone)-treated trypsin (1 μg/mL), to facilitate multi-cycle infection. All work on infectious SARS2 was carried out under strict biological safety level (BSL) 3 conditions at dedicated facilities within QUB, while work on IAV and EMCV was carried out under BSL2 conditions.

2.2. Methods

2.2.1. Preparation of the LDPE and 30 wt% TiO_2/LDPE Films

Two different plastic films were used in this work, namely, one comprising just LDPE, for blank experiments, and the other comprising LDPE with 30 wt% P25 TiO_2. A loading of 30 wt% P25 TiO_2 was used in this work, as other work, looking at the antibacterial activity of extruded P25 TiO_2/LPDE films, showed that the activity increased with increased loading of TiO_2 and that 30 wt% represented the highest loading achievable without compromising the film's tensile strength to such an extent that made large scale production difficult [37].

In the preparation of the latter, 6 g of P25 TiO_2 powder were mixed thoroughly with 14 g of the LDPE powder, and the mixture then fed into Rondol Microlab twin-screw extruder, which had a pre-heated mixing chamber set at 145 °C, and extruded as a 2.0 mm diameter filament, using an extruder screw speed of 70 rpm. This filament was subsequently cut up into 3 mm long pellets, which were then put through the extruder again under the same processing conditions. This re-feeding of the extruded pellets into the extruder was repeated a further two times to ensure the production of a fully blended 30 wt% TiO_2/LDPE masterbatch of pellets. The masterbatch pellets were then extruded under otherwise identical conditions described above, but through a slit die to generate a 30 wt% TiO_2/LDPE plastic film, rather than filament, which was ca. 30 μm thick. The plain LDPE film was generated using the same procedure as described above, but without the addition of the P25 TiO_2 powder.

A comparison of the physical properties of the TiO_2/LDPE and plain LDPE film is given in Section S1 in the electronic supplementary information (ESI) file. This includes, UV/Vis absorption spectra, water droplet contact angle values and tensile strength and Youngs modulus values.

2.2.2. UV Pre-Conditioning and Photocatalyst Testing

Previous work on extruded thin TiO_2/LDPE films has demonstrated that they exhibit little or no photocatalytic activity when used initially because the embedded TiO_2 particles are covered with the polymer which renders them effectively passive [37]. As a consequence, these films required 'activation' with UV radiation before they could be used to effect the photocatalytic destruction of the viruses under test. This UV pre-conditioning, activation step allows the TiO_2 particles at, or near, the surface to photocatalytically oxidise the thin layer of polymer covering them and so produce a photocatalytically active surface [37]. In the determination of the UV pre-conditioning time required to fully activate the TiO_2/LDPE film, *t*(UV activation), UV pre-conditioning was carried out using two, 352 nm UVA light (15 W BLB bulbs) with an incident irradiance of ca. 1.5 mW cm^{-2}.

The photocatalytic activity of each UV pre-conditioned, TiO_2/LDPE film was assessed initially by measuring its ability to bleach photocatalytically the dye, methylene blue, MB, dissolved in an aqueous

solution. This method of assessing photocatalytic activity was chosen as it is very similar to that of an international standard for assessing the activities of photocatalytic films [38].

In this work, a 12 × 8 mm^2 rectangular sample of the TiO_2/LDPE film under test was placed in a 1 cm pathlength cuvette, to which were then added 3.5 cm^3 of a 10 μM aqueous solution of MB, and the solution stirred continuously. The film was then irradiated with UVA (365 nm, 15 mW cm^{-2}) and, simultaneously, the photocatalysed bleaching of the MB monitored spectrophotometrically. A schematic illustration of the irradiation system, Fig. S4, and further details of the test are given in section S2 in the ESI file. From this work the initial rate of the photocatalysed bleaching of MB, r_i, was determined for each of the UV preconditioned TiO_2/LDPE films.

2.2.3. Virus Infectivity Assays

Each plastic film under test was stretched over a plastic ring (2.0 cm diameter), set in a square plastic base, and then fixed in place using a plastic outer ring to produce a sample 'drum' – in which the 'skin' was the UV conditioned plastic photocatalytic film under test. A schematic illustration of a typical drum is illustrated in Fig. S6(a) in the ESI. The photocatalytic plastic film 'skin' of the drum was then inoculated with 50 μL of the appropriate virus stock, with a concentration of ca. 1 × 10^7 infectious units/mL, and placed subsequently in the photocatalytic irradiation system, a schematic illustration of which is given in Fig. S6 (b) of the ESI. All irradiations of the virus inoculated photocatalytic plastic film drums were carried out using either two, 15 W 352 nm Black light blue (BLB) tubes or two, 15 W, cool white fluorescent tubes, which are commonly used in indoor lighting. The UV irradiances provided by the UV BLBs and cool white lamps were 1.5 mW cm^{-2} and 0.047 mW cm^{-2}, respectively; the cool white lamps provided a visible irradiance of 5000 lx. In the case of SARS2 only, all UV irradiations were carried out using just one 15 W 352 nm BLB tube to provide an irradiance of 0.25 mW cm^{-2}, whereas, as noted above, all the other viruses were irradiated with 1.5 mW cm^{-2} UV radiation. The emission spectra of the full cool white lamp and the UVA lamp used in this work are illustrated in Figs. S7 and 8, respectively in the ESI.

A UV irradiance of 1.5 mW cm^{-2} was chosen as a rough approximation of the UV irradiance associated with mid-day sunlight on an average, cloudy European day in April (total irradiance ca. 500 mW cm^{-2}), after passing through 3 mm glass window [39].

In the photocatalytic destruction of the different viruses, each sample was irradiated for a different time, i.e. 0, 0.25, 1, 2 or 3 h, and then removed and the inoculum, containing any remaining infectious virus, harvested from the material surface by rinsing with fresh cell culture medium, 200 μL of DMEM with high glucose. This virus-containing solution was then used to assess the level of viral infectivity remaining on the sample. Virus infectivity was determined by $TCID_{50}$ measurements in 96 well plates (IAV and EMCV) [40], or by plaque assay in 24 well plates (SARS2) using a method described elsewhere [36], except modified using VAT cells and incubating infections for 48 h prior to determining the number of plaque forming units, PFU, produced. Calculated virus infectivity values were based on visual viral cytopathic effect measurements (WSN, EMCV and SARS2), or on red fluorescence measurements for PR8 using a Celigo cytometer. Each assessment was carried out three times and the typical error in the log of the measured infectivity values was ±0.38.

2.2.4. Other Methods

In all the MB photocatalytic studies reported here a 2.8 W, 365 nm UVA LED (RS, Corby, UK), was used as the UV source. All UV irradiances were measured using a Hamamatsu UV power meter. All UV/Vis absorption spectra, including those of the MB reaction solution, were recorded using Cary 60 UV/Vis spectrophotometer (Varian, Santa Clara, USA). SEM images were acquired using a recorded field-emission gun scanning electron microscope, i.e. FEG-SEM, (JEOL JSM-6500F). Water droplet contact angle measurements were made using a FTA32 instrument (First Ten Angstrom, Newark, USA), in which each of the sample films was stuck to a microscope slide using double sided tape and a 6 μL water droplet was then deposited onto the sample's surface. From the captured images of the water droplet, the FTA32 software was used to calculate the water droplet contact angle. Each sample was tested in this way five times and the average value reported.

3. Results and Discussion

3.1. UV Pre-Conditioning

As noted earlier, previous work on extruded thin TiO_2/LDPE films showed that they need to be activated via a UV conditioning step before they could be used as photocatalytic films [37]. In order to identify how long the 30 wt% TiO_2/LDPE film used in this work film needed to be UV conditioned for it to be fully activated, a study was carried out in which samples of the TiO_2/LDPE film were UV conditioned for a variety of different times and then tested for activity using a method, based on the photocatalysed bleaching of MB, which is also the basis of a well-established International Standards Organisation, ISO, test method [38,41]. In the test, the overall process can be best summarised as follows,

$$\mathrm{MB} + n\mathrm{O_2} \xrightarrow[\mathrm{UVA}]{\mathrm{TiO_2}} \text{colourless products} \quad (1)$$

and details of the method employed are given in 2.2.2 of the Experimental section and S2 in the ESI.

In each case, a [MB] vs irradiation time, *t*, plot was generated from which a value for the initial rate of photobleaching of MB, r_i, was determined. The latter is a measure of the activity of the photocatalytic film under test and a plot of the measured variation in r_i with UV-preconditioning time, arising from this work, is illustrated in Fig. 3. These results show that the 30 wt% TiO_2/LDPE film is initially rendered increasingly active photocatalytically with increasing UV preconditioning time, but that after just 60 h UV pre-conditioning, the photocatalytic activity of the film appears to have reach a maximum value. The apparent maximum rate of reaction (1) of 0.38 μM min^{-1} exhibited by the 30 wt% TiO_2/LDPE film UV preconditioned for ≥60 h is most likely due to mass transport control, and so limited by the rate of diffusion of the MB from the bulk of the reaction solution to the surface of the photocatalytic plastic film. This is not too surprising, since mass transport is a recognized problematic feature of this test in the assessment of very active films [42].

In a study of the MB ISO [38], Tschirch et al. have estimated [42] the initial diffusion-controlled rate in such a system, r_D, is given by the following expression,

r_D (units: μM min^{-1}) = 0.06.D_{MB}.[MB].A/(b.V) (2)

where, D_{MB} is the diffusion coefficient for MB (6.74 × 10^{-6} cm^2 s^{-1}) [43], [MB] is the initial bulk concentration of MB (10 μM in this work), A is the photocatalyst surface area (1 cm^2), b is the diffusion layer thickness, which is ca. 100 μm for a stagnant aqueous solution [44], and V is the reaction solution volume (3.5 × 10^{-3} dm^3). Using this equation, and the above values for the various parameters used in this work, a value for r_D of 0.38 μM min^{-1} can be generated for our MB test system conducted using a 1 cm cuvette as the reactor, assuming a value for b of ca. 32 μm, which appears reasonable, given the reaction solution is not stagnant but rather vigorously stirred.

Indirect evidence that UV pre-conditioning of the 30 wt% TiO_2/LDPE film roughens the surface and exposes the underlying TiO_2 photocatalyst particles, is provided by the measured change in water droplet contact angle, CA, exhibited by the TiO_2/LDPE film as a function of UV preconditioning time, the results of which are also illustrated in Fig. 3. LDPE is a hydrophobic material, with a water droplet contact angle of ca. 80°, whereas P25 TiO_2, is highly hydroxylated, and superhydrophilic, i.e. with a CA value of <10° [45]. As a result, as more and more TiO_2 photocatalytic particles are exposed with increasing UV pre-

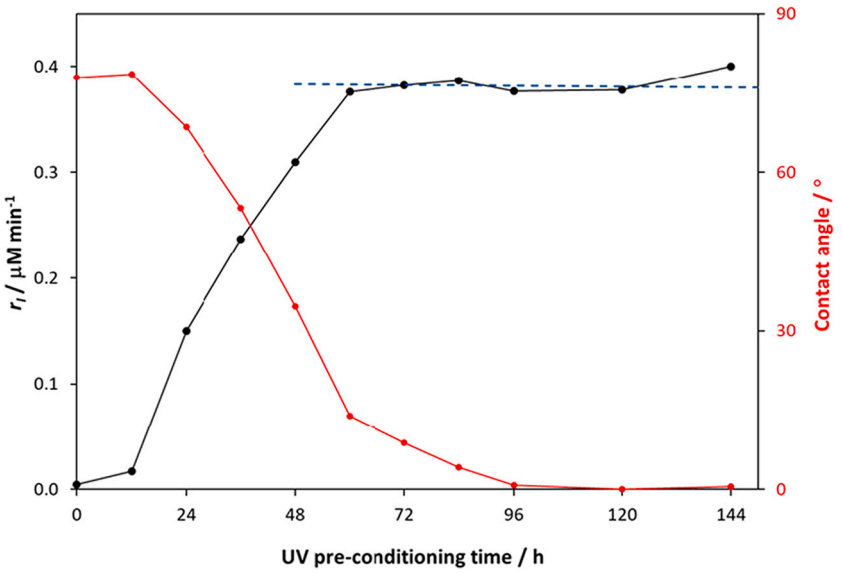

Fig. 3. Plot of the initial rate of bleaching of MB (black line), r_i, and measured water droplet contact angle (red line), as a function of UV pre-conditioning time for a 30 wt% TiO_2/LDPE film. The broken line represents the average maximum rate (0.38 µM min^{-1}) from 60 to 144 h UV preconditioning. (For interpretation of the references to colour in this figure legend, the reader is referred to the web version of this article.)

conditioning it is expected that the measured value of the CA of the TiO_2/LDPE film would decrease significantly. The observed variation in CA with UV pre-conditioning time for these films illustrated in Fig. 3 confirms this expected feature, with CA decreasing from an initial value of ca 80^o to ca. 0^o after 144 h exposure to 1.5 mW cm^2 UVA radiation.

Direct evidence of the significant disruption of the surface and TiO_2 photocatalyst particle exposure brought about by UV pre-conditioning is provided by scanning electron microscopy, SEM, and an illustrative sample of the micrographs recorded of the UV pre-conditioned TiO_2/LDPE films, are illustrated in Fig. 4.

The images in Fig. 4 provide direct evidence of the surface disruption, accompanied by TiO_2 particle exposure, effected by UV pre-conditioning the TiO_2/LDPE film. Higher resolution SEM images of these films are given in Fig. S9 of the ESI. These images are similar to those reported by Lam et al. in their study of the effect on sunlight on films of LDPE doped with photocatalytic particles of ZnO and Fe-ZnO

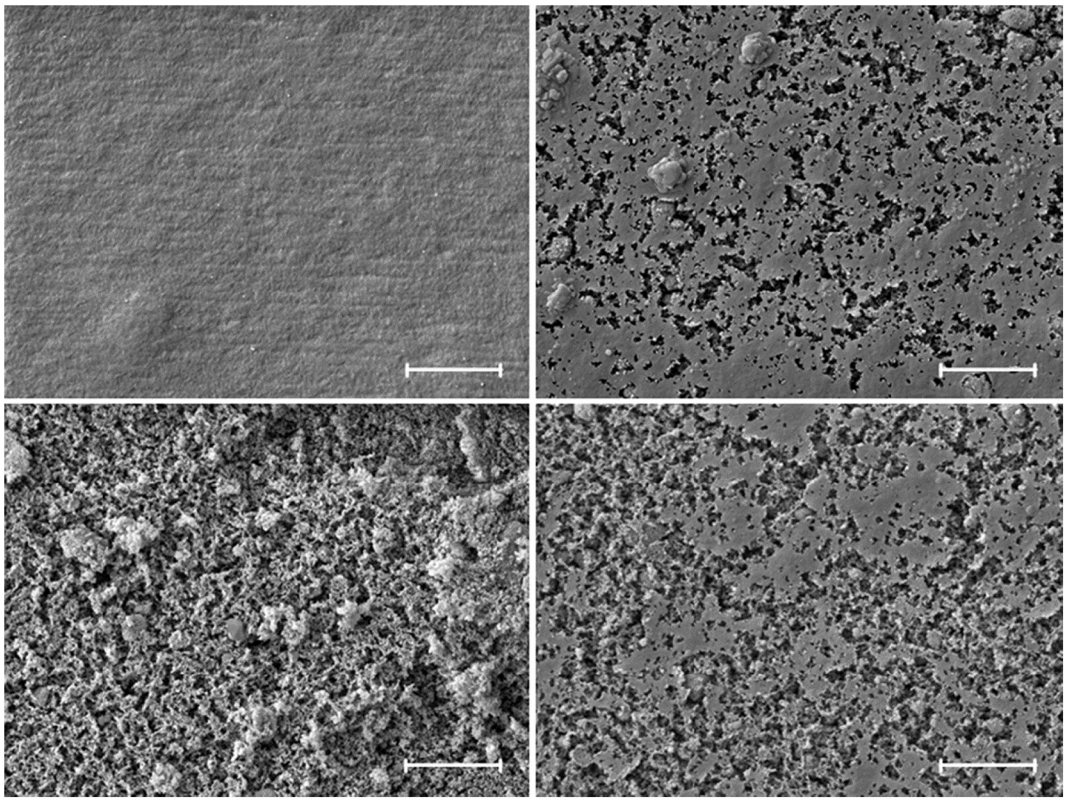

Fig. 4. Scanning electron micrographs of the TiO_2/LDPE film UVA pre-conditioned (1.5 mW cm^{-2}) for (clockwise starting from top left), 24, 36 72 and 144 h, respectively. The white bar in each image represents 5 µm. UV pre-conditioning irradiance, 352 nm, 1.5 mW cm^{-2}).

[29] and reflect the ability of these particles, as with those of TiO_2, to degrade the encapsulating polymer.

Interestingly, although the plot of initial rate vs UV pre-conditioning time, *t*, suggests the rate is maximal after 60 h pre-irradiation, see Fig. 3, the variation in CA vs UV pre-conditioning time profile, also illustrated in Fig. 3, suggests that the number of particles of TiO_2 exposed by the UV pre-conditioning process continues to increase after $t = 60$ h, and that the most active surface, with a CA value of 0^o, is only achieved with $t \geq 120$ h. The further disruption of the surface of the TiO_2/LDPE film with *t* values ≥60 h is also very apparent from the SEM images of the films illustrated in Fig. 4. Therefore, in order to ensure that the UV pre-conditioned TiO_2/LDPE film used to destroy viruses had the highest activity, a UV pre-condition time of 144 h was used to activate the 30 wt % TiO_2/LDPE film used in all the work on viruses.

An obvious conclusion that one must draw from the results of this work, and that of others [28,29], is that, with prolonged UV pre-activation, or use, a TiO_2/LDPE plastic film will eventually disintegrate. However, other work shows that even after 300 h UV pre-conditioning, the TiO_2/LDPE continues to be just as effective in photocatalysing the oxidative bleaching of MB, i.e. reaction (1), as a 144 h pre-conditioned film. Evidence that a 144 h UV pre-conditioned TiO_2/LDPE film does not readily lose its activity with prolonged use was provided by using the same film to photocatalyse reaction (1) five times in succession, the results of which are shown in Fig. 5 in the form of the recorded variation in the absorbance due to the MB at 665 nm, ΔAbs_{665}, vs irradiation time, *t*. The decay profiles illustrated in Fig. 5 are very similar and show no evidence of decreasing activity with use, which suggests that the 144 h UV pre-conditioned (352 nm, 1.5 mW cm^{-2}) TiO_2/LDPE film is robust both photocatalytically and physically, even after exposure to intense UV radiation (365 nm, 15 mW cm^{-2}) for a further 15 h. It also should be remembered that the most likely use of such photocatalytic plastic films is as a low cost, added value (in that they are now self-sterilising), alternative to current disposable plastic films, often used extensively in the healthcare industry for example, and that as such they would now usually be used for <1 day before being thrown away.

Additional evidence of the physical robustness of the 144 h UV pre-conditioned, 30 wt% TiO_2/LDPE film was provided by comparing the measured initial rate of photocatalyzed oxidation of MB, i.e. reaction (1), of the film before and after it was subjected to the 3 M Scotch Tape test [46]. In this test a piece of tape is stuck to the film under test and then peeled off, along with any weakly adhering coating. Although the 30 wt% TiO_2/LDPE film was only 30 μm thick, and the tape is 60 μm thick, the photocatalytic film was undamaged when subjected to the 3 M Scotch Tape test and its activity, as measured using the MB test described above, was almost identical, i.e. 92% of the original, which suggests that the photocatalytic coating in a 144 h UV pre-conditioned, 30 wt% TiO_2/LDPE film is physically robust.

3.2. Destruction of Viruses on Activated TiO_2/LDPE Films Using UV Radiation

The photocatalysed inactivation of SARS2, EMCV, WSN and PR8 by a 144 h UV pre-conditioned TiO_2/LDPE plastic film using UV radiation was studied using an irradiance = 1.5 mW cm^{-2} for all viruses except SARS2 (0.25 mW cm^{-2}). As noted earlier a UV irradiance of 1.5 mW cm^{-2} was chosen to approximate that associated with sunlight after having passed through a glass window. The results of this work, in the form of log[virus] vs irradiation time, *t*, profiles are illustrated in Fig. 6, along with those recorded for the same systems where no UV light was used, i.e. in the dark.

These results show that for each of the 4 viruses tested, the active concentration was reduced to a very low level (< 1 log(PFU/$TCID_{50}$) within 2 h irradiation. This indicates the UV precondition TiO_2/LDPE plastic film could act as a very effective, self-sterilising film under approximate sunlit room conditions. Interestingly, from the decay profiles illustrated in Fig. 6, it appears that in the dark, the UV pre-conditioned 30 wt% TiO_2/LDPE film exhibits some ability to inactivate all four viruses, most notably SARS2 and PR8. This, albeit limited, antiviral activity may be due to the nm/μm roughness of the 144 h UV pre-conditioned TiO_2/LDPE film, illustrated in Fig. 4. A high-resolution SEM image of this film is illustrated in Fig. S10 in the ESI and highlights the significant roughness on the nm scale that is most likely responsible for its modest dark antiviral activity with regard to SARS2 and PR8. It is known that rough surfaces, especially those with features similar in size to that of the virions, in this case 30–100 nm, are able to act as a 'bed of nails' and physically damage them [47–51]. The typical reduction in log [virus] levels by 1–2 over 3 h, observed for all 4 viruses on the UV pre-conditioned TiO_2/LDPE in the *dark*, see Fig. 6, is similar to that reported for respiratory syncytial virus and rhinovirus inocula when deposited on aluminum films with nanostructured surfaces produced by etching [51].

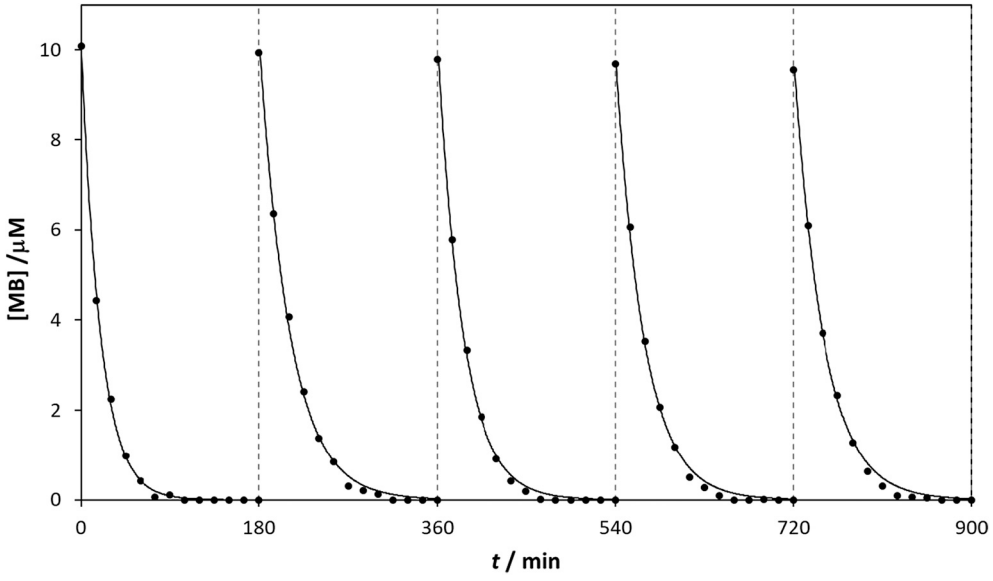

Fig. 5. Plot of ΔAbs_{665} vs irradiation time recorded for the same 144 h UV pre-conditioned TiO_2/LDPE film (1 cm^2) when used to photocatalyse the bleaching of an aqueous MB solution (3.5 cm^3; 10 μM) via reaction (1), using 365 nm radiation (15 mW cm^{-2}) five times in series. Average initial rate for each decay is 0.38 μM min^{-1}.

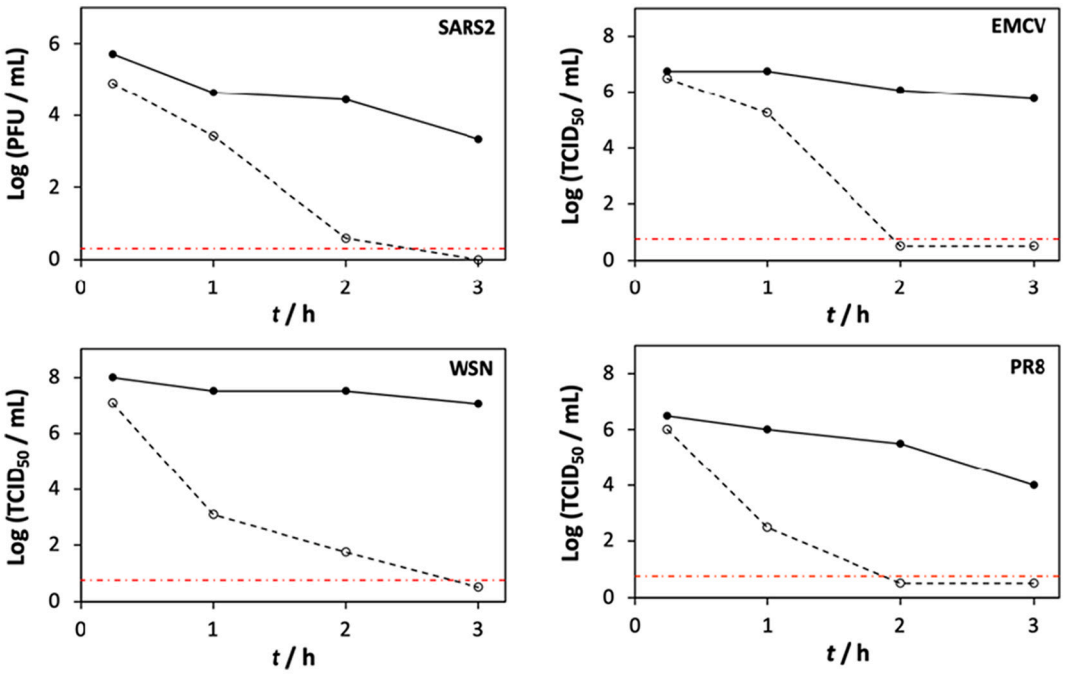

Fig. 6. Photocatalysed inactivation vs irradiation time profiles recorded for four different viruses using a 144 h UV pre-conditioned TiO_2/LDPE plastic film and UV radiation (open circles). The closed circles data points were determined for the same systems but with no UV irradiation. The long-dashed red horizontal lines highlight the lower limits of reliable detection. (For interpretation of the references to colour in this figure legend, the reader is referred to the web version of this article.)

It is well-know that UV irradiation can damage the RNA/DNA in most viruses and, by doing so, inactive them [52–54]. Such UV inactivation is possible because the conjugated double bonds in their purine and pyrimidine rings have a specific absorption peak at 260 nm. As a result, UVC (280–200 nm [55]) radiation can be particular effective in inactivating viruses, but, as nucleic acids absorb little above 340 nm, the 365 nm UVA radiation used in this work, or the cool white light for that matter, is unlikely to produce any significant inactivation of the viruses via the electronic excitation of their genetic material, unless they are particularly sensitive. Indeed, a recent study of the UV action spectrum for the deactivation of SARS2 revealed 278 nm radiation (UVC) was ca. 10,000 times more effective than either 365 (UVA) or 405 (visible) nm radiation [56].

When the four viruses were tested on plain LDPE, some loss of infectivity was observed with irradiation time for the SARS2, WSN and PR8 viruses, as indicated by the relevant log(PFU/$TCID_{50}$) vs UV

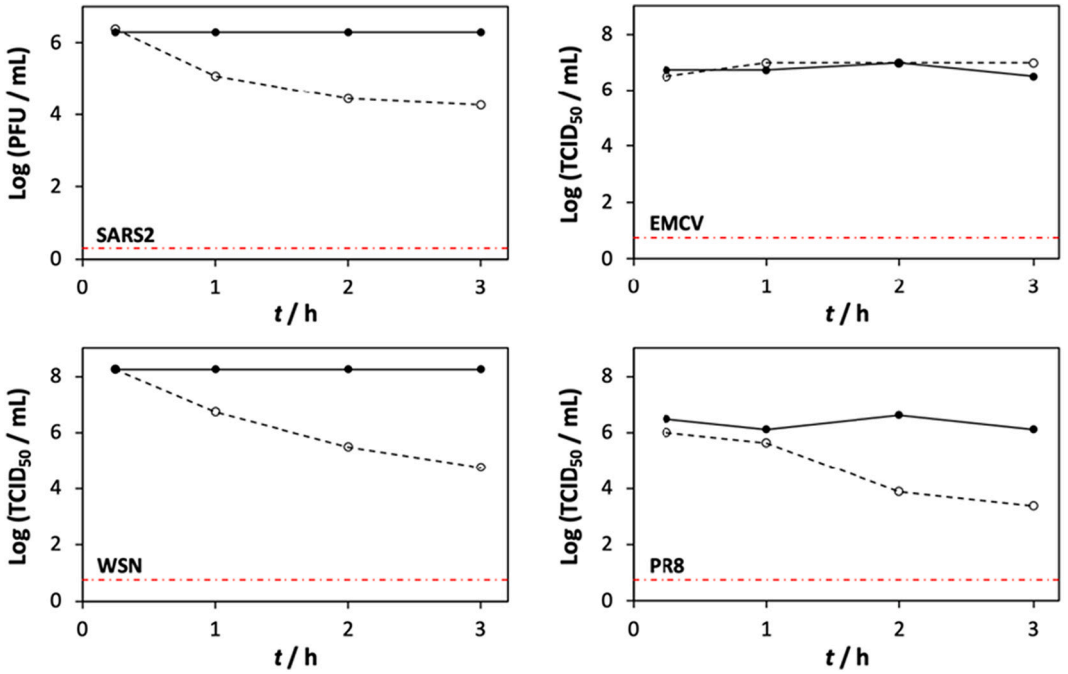

Fig. 7. Measured log(PFU/$TCID_{50}$) vs irradiation time, *t*, profiles recorded for four different viruses deposited on just a LDPE plastic film and UV radiation, (open circles). The closed circles data points were determined for the same systems but with no UV irradiation.

irradiation time, *t*, profiles illustrated in Fig. 7. The loss of activity exhibited by SARS2 is particularly striking given that all UV irradiations of SARS2 were carried out using an irradiance (0.25 mW cm^{-2}), which was 6 x's lower than that used with all the other viruses (1.5 mW cm^{-2}). This striking loss would seem to suggest that SARS2 is very sensitive to UVA radiation, and yet the recent UV action spectrum study showed that SARS2 is much more stable than other RNA viruses, such as IAV, when exposed to UVA radiation and that a 2 log reduction in SARS2 loading would require at least 12 h irradiation with 0.25 mW cm^{-2} UVA, not the apparent 3 h observed here, see Fig. 7 [56]. A likely major contributor to the loss of infectivity exhibited by the influenza A viruses, WSN and PR8, is the incident UV radiation which can cause damage in viral lipids, proteins and RNA. Support for this is provided by the much-reduced decay profiles exhibited by these same two viruses (but not by SARS2) on LDPE under visible light irradiation, see Fig. S8 in ESI.

The cause of the loss infectivity in SARS2, and a contributor to that exhibited by the WSN and PR8 viruses, on LDPE and when exposed to UV or visible light on LDPE, is most likely the heat emitted by the lamps, which produced a small increase in the ambient temperature (by ca. 2 °C by the UVA lamps and ca. 1.5 °C by the visible lamps and the 0.25 mW cm^{-2} UVA irradiation system, with room temperature = ca. 17.5 °C). This is perhaps not too surprising given heat treatment is a widely used method for inactivating viruses and is thought to work by denaturing the secondary structures of proteins and other molecules like the lipid envelope, resulting in impaired molecular function, in particular the ability to bind and enter the host cells. [54,57,58]. A previous study shows that that SARS2 can be rendered inactive by heat by holding it at 56 °C for 30 min, or 95 °C for 3 min [59]. It follows in this work that, if the heat of the lamps does effect some loss of viral activity, the small temperature increase produced by irradiating sample, must be rendered effective due by the significant exposure time, i.e. 3 h.

In contrast to the other 3 viruses, the infectivity of EMCV on LDPE appears unaffected under UVA and visible light irradiation, which indicates it is neither sensitive to the heat of the lamps or UV radiation-induced damage. All 4 viruses on LDPE film were very stable in the dark, as expected given its smooth and chemically inert nature.

A simple summary of the anti-viral activity exhibited by the 30 wt% TiO_2/LDPE film with, and without, irradiation with UVA and that of the LDPE film, with UV irradiation, is provided the average rate of inactivation (i.e. $\Delta\log[virus]/\Delta t$) for each virus, under these three different conditions. The value of $\Delta\log[virus]/\Delta t$ was calculated for each of the decay profiles illustrated in Fig. 6 by first using the decay profile to estimate values for the irradiation times at which log[virus] was equal to 4 and 1, i.e. t_4 and t_1, respectively and where this was possible, the value of the average rate, $\Delta\log[virus]/\Delta t$, was calculated as follows,

$$\Delta\log[virus]/\Delta t = 3/(t_1 - t_4) \quad (3)$$

However, for the many cases when the log[virus] level didn't fall to ≤1 over the 3 h period, such as in all the decay profiles illustrated in Fig. 7, eq. (3) is inappropriate, and so in these cases the average rate was estimated over the whole decay, using the follow expression,

$$\Delta\log[virus]/\Delta t = -(\log[virus]_{3.0} - \log[virus]_{0.25})/2.75 \quad (4)$$

where, $\log[virus]_{3.0}$ and $\log[virus]_{0.25}$ were the measured values of log[virus] at irradiation times 3 h and 15 min, respectively, taken from the relevant decay plots in Figs. 6 and 7.

A histogram plot of the average rates, based on the decay plots illustrated in Figs. 6 and 7 and calculated using eq. (3) or (4) as described above, is illustrated in Fig. 8 and reveals that in the UV illumination of the virus-coated, 30 wt% TiO_2/LDPE film the order of virus inactivation average rates is as follows, EMCV > > PR8, SARS2 > WSN and that, when compared to no UV irradiation, the ratio of the rates was 13.2, 4.6, 3.1 and 3.0 for EMCV, WSN, PR8 and SARS2, respectively, indicating a significant, sometimes very significant (as in the case of EMCV), UV-driven, photocatalytic anti-viral effect.

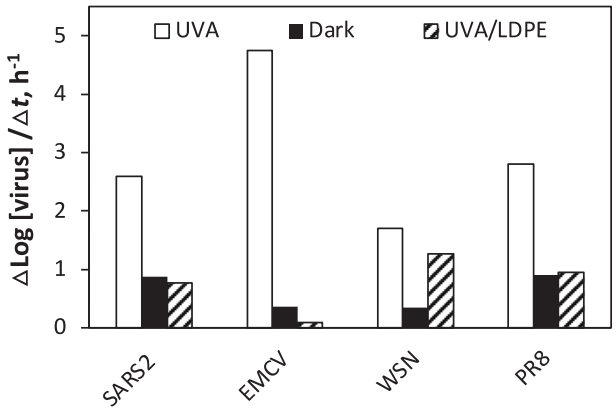

Fig. 8. Histogram plot of the calculated average inactivation rates for the 4 different viruses, for the (i) 30 wt% TiO_2/LDPE film with UVA, (ii) 30 wt% TiO_2/LDPE film without UVA, and (iii) LDPE film with UVA. In this work the UVA (365 nm) irradiance used was, 1.5 mW cm^{-2} for all but SARS2 (0.25 mW cm^{-2}).

3.3. Destruction of Viruses on Activated TiO_2/LDPE Films Using Cool White Light

The photocatalysed inactivation of SARS2, EMCV, WSN and PR8 by a 144 h UV pre-conditioned TiO_2/LDPE plastic film was also studied using a cool white light source, comprising two, 15 W cool white fluorescent tubes) radiation, UV irradiance = 0.047 mW cm^{-2}, which was chosen to simulate a well-lit room. The log[virus] vs *t* profiles generated for the 4 different viruses, on the UV pre-conditioned TiO_2/LDPE film, with and without cool white light irradiation, are illustrated in Fig. 9 and show that for each of the 4 viruses tested, the active concentration was reduced significantly over the 3 h irradiation period. Thus, it appears that the UV preconditioned TiO_2/LDPE plastic film could act as a very effective self-sterilising film in a room well-lit with cool white fluorescent lamps.

When the four viruses were tested on plain LDPE and irradiated with cool white light, once again SARS2 exhibited a noticeable loss of activity, as indicated by the relevant log(PFU/$TCID_{50}$) vs UV irradiation time, *t*, profiles illustrated in Fig. S11 in the ESI. This loss in activity is almost the same as exhibited by SARS2 when irradiated with UVA radiation, see Fig. 7, which suggests that both are primarily due to thermal (rather than UV-induced) deactivation. In contrast, WSN and PR8 on LDPE exhibited much reduced losses in activity when irradiated with cool white light compared to UVA light, suggesting UV-induced deactivation is significant on plain LDPE. Finally, once again, EMCV on LDPE appeared largely unaffected when irradiated, i.e. it is stable both in visible and UV light. To aid the above comparisons, the visible and UV light decays exhibited by the four viruses on plain LDPE are illustrated in Fig. S12 in the ESI.

A simple summary of the anti-viral activity exhibited by the 30 wt% TiO_2/LDPE film with and without irradiation with a cool white light (UVA irradiance = 0.047 mW cm^{-2}) and that of the LDPE film, with the same cool white light irradiation, is provided by the histogram of the calculated average rate (i.e. $\Delta\log[virus]/\Delta t$) for each virus, based on eq. (3) or (4), illustrated in Fig. 10.

This plot shows that in the case of the cool white light illumination of the 30 wt% TiO_2/LDPE film, the order of virus inactivation activity average rates is, PR8 > > SARS2 > WSN,EMCV and that when compared to no UV irradiation, the ratio of the rates was 4.5, 4.4, 4.3 and 2.3 for WSN, PR8, EMCV and SARS2, respectively, indicating, once again, a significant photocatalytic effect for all 4 viruses.

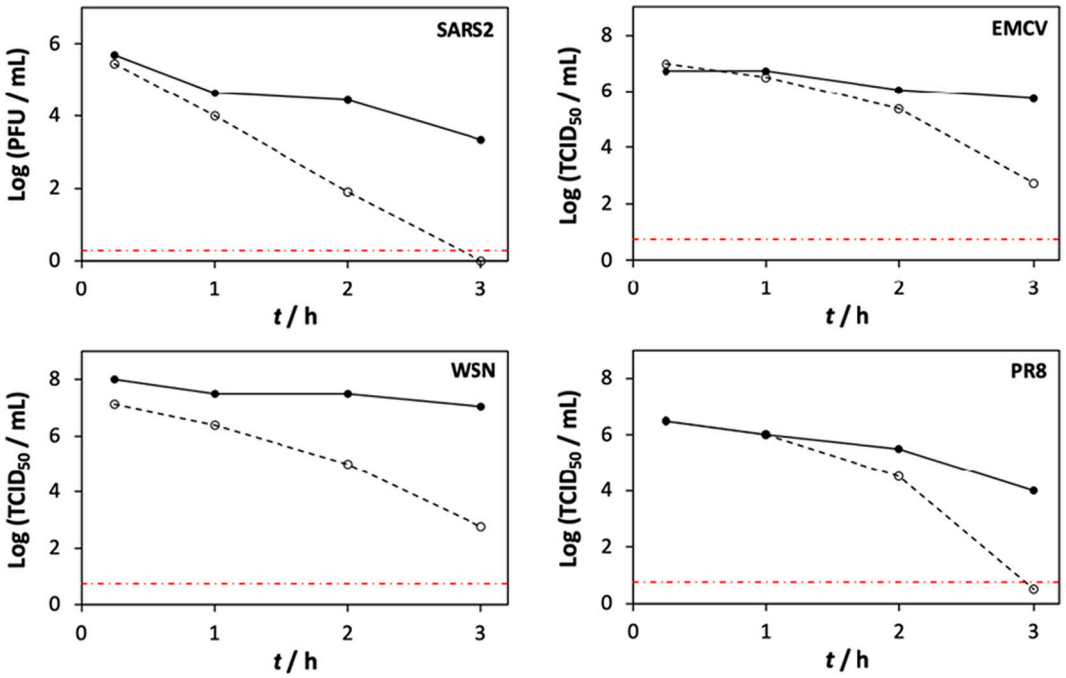

Fig. 9. Photocatalysed inactivation vs irradiation time profiles recorded for the four different viruses using a 144 h UV pre-conditioned TiO_2/LDPE plastic film and cool white light, UV irradiance = 0.047 mW cm^{-2} (open circles). The closed circles data points were determined for the same systems but with no irradiation, i.e. in the dark.

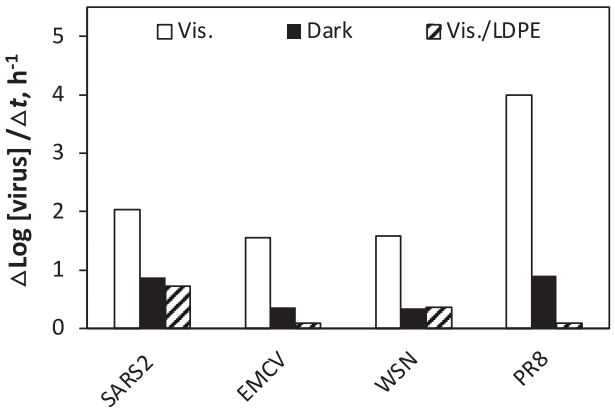

Fig. 10. Histogram plot of the calculated average inactivation rates for the 4 different viruses, for the (i) 30 wt% TiO_2/LDPE film with cool white light (CWL) irradiation, (ii) 30 wt% TiO_2/LDPE film without irradiation, and (iii) LDPE film with CWL irradiaation. In this work the UVA (365 nm) irradiance from the CWL was, 0.047 mW cm^{-2}.

3.4. Comparison of Photocatalytic Inactivation Rates

When the two histograms of average rate are compared, i.e. Figs. 8 and 10, there is no obvious correlation between the two irradiation-induced inactivation rates, and so the ratio of UV and cool white rates for EMCV, SARS2, WSN and PR8, are dissimilar, i.e. 3.1, 1.3, 1.1 and 0.70, respectively. However, for SARS2, WSN and PR8, it is striking how little, if at all, the average rate is increased when the TiO_2/LDPE films are exposed to a significant level of UV irradiation ($\rho = 1.5$ mW cm^{-2}, or 0.25 mW cm^{-2}), compared to when they are irradiated with cool white lamps, with its much more modest UV irradiance component, $\rho = 0.047$ mW cm^{-2}. This observation is not too surprising in that the rate of photocatalysis is often found to depend upon $\rho^{0.5}$ at high UV irradiances and ρ at low values [21]. This feature also helps explain why several research groups have reported [14,15,17,60] significant photocatalytic virus inactivation under just room light conditions, where the UV irradiance is expected to be similar to that reported here for cool white lamps.

Finally, it is useful to compare and contrast the photocatalytic virus inactivation rates reported here with those reported in the literature for other photocatalytic films, i.e. dry TiO_2 powder, colloid or sol-gel coatings on an inert support substrate, using similar viruses. Thus, Table 1 lists key details of these films, including average inactivation rate values and light sources, alongside the results reported here [12,16,17,61,62]. A brief inspection of the values of $\Delta\log[\text{virus}]/\Delta t$ reported for SARS2 and IAV inactivation in Table 1, indicate that the 30 wt% TiO_2/LDPE film is more effective than the other cited photocatalytic films.

The reported photocatalyzed inactivation of the human rotavirus strain Odelia using a TiO_2 film of particles on a fluorocarbon is slow compared to that of SARS2 or influenza [63], which is consistent with the fact that it is, unlike the latter, non-enveloped and so more stable. However, the noted general stability of non-enveloped viruses does not appear to extend to the photocatalytic inactivation of EMCV, when using the 30 wt% TiO_2/LDPE film, as indicated by the results in Table 1. The apparent greater stability of the rotavirus, compared to EMCV, a picornavirus, maybe be because the former has multiple capsid shells, whereas the latter does not [63,64].

The results given in Table 1 suggest that the UV pre-conditioned 30 wt% TiO_2/LDPE film used here is effective in inactivating enveloped and non-enveloped viruses, and exhibits an activity that is generally much greater than those reported previously for TiO_2 films, using either UVA or white fluorescent light sources. In addition, in contrast to the other films in Table 1 and most examples of anti-viral photocatalytic TiO_2 films per se, the 30 μm thick, 30 wt% TiO_2/LDPE film is very flexible and physically robust, which suggests that it could play a significant role in the healthcare industry as a disposable, active self-sterilising plastic film which functions well in both room light and window-glass filtered sunlit conditions.

Table 1
Reported TiO_2-based photocatalytic inactivation rates [12,16,17,27,61,62].

Virus	Substrate	Light source	Irradiance (mW cm^{-2})	△Log [Virus] /△t, h^{-1}		Ref.
				TiO_2 film	Substrate	
SARS2	Glass fibre sheet (Powder)	LED light (405 nm)	1.0	1.50	0.35	[16]
SARS2	Ceramic tiles (Powder)	White FL.	610 lx	0.88	–	[17]
SARS2	LDPE (Powder)	UVA (352 nm)	0.25	2.60	0.77	**This work**
		White FL.	0.047	2.03	0.73	
Influenza (PR8)	Glass (Colloid)	UVA (352 nm)	1.0	1.25	–	[12]
Influenza (H_9N_2)	Glass (Sol-gel)	UVA (365 nm)	1.5	1.33	0.47	[27]
Influenza (PR8)	Glass (Colloid)	UVA (352 nm)	0.1	0.90	0.10	[61]
Influenza (PR8)	LDPE (Powder)	UVA (352 nm)	1.5	2.81	0.95	**This work**
		White FL.	0.047	4.00	0	
Influenza (WSN)	LDPE (Powder)	UVA (352 nm)	1.5	1.70	1.27	**This work**
		White FL.	0.047	1.59	0.36	
Rotavirus (Odelia)	Fluoroplastic (Powder)	White FL.	2900 lx	0.06	0.01	[62]
EMCV	LDPE (Powder)	UVA (352 nm)	1.5	4.75	0	**This work**
		White FL.	0.047	1.55	0.09	

4. Conclusions

A thin, 30 μm, flexible, robust LDPE film, loaded with P25 TiO_2, once activated using a UV pre-conditioning step, is able to effect the inactivation of a range of different viruses, including SARS2. The average rate of the photocatalysed inactivation of SARS2 is only 1.3 x's faster when using a dedicated, low intensity UVA source (0.25 mW cm^{-2}) compared to a cool white lamp (UVA irradiance = 0.047 mW cm^{-2}), which suggests the virus is particularly prone to inactivation by photocatalysis and that the film will be effective in a room lit with just white fluorescent tubes. The film is produced by extrusion, a common, large-scale process, using very inexpensive materials. Although, at present, a long (144 h) UV pre-conditioning step is required to render it photocatalytically active, this time might be reduced significantly by using UVC, rather than UVA radiation, as it is absorbed much more strongly (ca. 10 x's) and/or by using a much greater UV irradiance, i.e. $>>$ 1.5 mW cm^{-2}. It may also be possible to activate these films using an alternative approach, such as plasma treatment, which is a common, large-scale process used to treat hydrophobic polymers, such as polyethylene, to improve their wettability, since it damages the surface of the polymers in a similar way as does photocatalysis and so should expose the photocatalyst particles. Both approaches to fast activation are currently under investigation. If the activation of photocatalyst-loaded, extruded thin, flexible plastic films can be readily carried out via a scalable, inexpensive process, then it is likely to lead to a new commercial product range, namely, inexpensive, self-sterilising, flexible, robust, plastic films, which is likely to find many applications, including as an added-value disposable plastic film for use in the health-care industry. The need for a UV-activation step is clearly a negative feature of this film and other negative features include that it is UV driven and less strong and elastic than plain LDPE, see S1 in ESI. Both these negative features would be readily overcome if a visible light-absorbing, active, low cost alternative to TiO_2 could be identified, since it would utilise much more of the ambient light and by so doing would require use at much a lower loading level. The current dominance of TiO_2 in all commercial examples of photocatalytic films (such as tiles, glass, paint and fabric) highlights the fact that such an alternative photocatalyst has yet to be found. The thin, plastic, self-sterilising photocatalytic film reported here has potential as a new commercial photocatalytic product, but, like all current photocatalytic products, is likely to be markedly improved if a suitable visible light absorbing alternative photocatalyst can be found.

Data access statement

All data is provided in full in the results section of this paper and supplementary information accompanying this paper.

CRediT authorship contribution statement

Ri Han: Investigation, Visualization, Writing – original draft. **Jonathon D. Coey:** Investigation, Visualization, Writing – original draft. **Christopher O'Rourke:** Investigation, Visualization. **Connor G.G. Bamford:** Conceptualization, Supervision, Writing – original draft. **Andrew Mills:** Writing – original draft, Conceptualization, Supervision, Writing – review & editing.

Declaration of Competing Interest

The authors declare that they have no known competing financial interests or personal relationships that could have appeared to influence the work reported in this paper.

Acknowledgements

This work was funded by the EPSRC (EP/V041541/1).

Appendix A. Supplementary data

Supplementary data to this article can be found online at https://doi.org/10.1016/j.jphotobiol.2022.112551.

References

[1] N. Castano, S.C. Cordts, M. Kurosu Jalil, K.S. Zhang, S. Koppaka, A.D. Bick, R. Paul, S.K.Y. Tang, Fomite transmission, physicochemical origin of virus-surface interactions, and disinfection strategies for enveloped viruses with applications to SARS-CoV-2, ACS Omega 6 (2021) 6509–6527, https://doi.org/10.1021/acsomega.0c06335.
[2] N.H.L. Leung, Transmissibility and transmission of respiratory viruses, Nat. Rev. Microbiol. 19 (2021) 528–545, https://doi.org/10.1038/s41579-021-00535-6.
[3] S.A. Boone, C.P. Gerba, Significance of fomites in the spread of respiratory and enteric viral disease, Appl. Environ. Microbiol. 73 (2007) 1687–1696, https://doi.org/10.1128/aem.02051-06.
[4] D.R. Eddy, M.D. Permana, A. Lutfiah, A.R. Noviyanti, Y. Deawati, I. Rahayu, Challenges of TiO2-composite, as a visible active photocatalyst material for Sars-Cov-2 antiviral compared with the other viruses, Quim Nova 45 (2021) 74–82, https://doi.org/10.21577/0100-4042.20170807.
[5] N.V. Doremalen, T. Bushmaker, D.H. Morris, M.G. Holbrook, A. Gamble, B. N. Williamson, A. Tamin, J.L. Harcourt, N.J. Thornburg, S.I. Gerber, J.O. Lloyd-Smith, E.D. Wit, V.J. Munster, Aerosol and surface stability of SARS-CoV-2 as compared with SARS-CoV-1, N. Engl. J. Med. 382 (2020) 1564–1567, https://doi.org/10.1056/NEJMc2004973.
[6] N. Lin, D. Verma, N. Saini, R. Arbi, M. Munir, M. Jovic, A. Turak, Antiviral nanoparticles for sanitizing surfaces: a roadmap to self-sterilizing against COVID-19, Nano Today 40 (2021), 101267, https://doi.org/10.1016/j.nantod.2021.101267.
[7] Pilkington, Self-cleaning Glass. https://www.pilkington.com/en-gb/uk/households/types-of-glass/self-cleaning-glass. Accessed April 2022.
[8] TAIYO, Europe. https://taiyo-europe.com/materials/pvc/. Accessed April 2022.
[9] IKEA, Purify your air with GUNRID curtains. https://www.ikea.com/sa/en/rooms/living-room/how-to/purify-your-air-with-gunrid-curtains-pubc73769b0. Accessed April 2022.

[10] Hytect. https://hytect.com/en. Accessed April 2022.
[11] STO. https://www.sto.co.uk. Accessed April 2022.
[12] R. Nakano, H. Ishiguro, Y. Yao, J. Kajioka, A. Fujishima, K. Sunada, M. Minoshima, K. Hashimoto, Y. Kubota, Photocatalytic inactivation of influenza virus by titanium dioxide thin film, Photochem. Photobiol. Sci. 11 (2012) 1293–1298, https://doi.org/10.1039/C2PP05414K.
[13] P. Hajkova, P. Spatenka, J. Horsky, I. Horska, A. Kolouch, Photocatalytic effect of TiO2 films on viruses and bacteria, Plasma Process. Polym. 4 (2007) S397–S401, https://doi.org/10.1002/ppap.200731007.
[14] G.W. Park, M. Cho, E.L. Cates, D. Lee, B.T. Oh, J. Vinje, J.H. Kim, Fluorinated TiO2 as an ambient light-activated virucidal surface coating material for the control of human norovirus, J. Photochem. Photobiol. B 140 (2014) 315–320, https://doi.org/10.1016/j.jphotobiol.2014.08.009.
[15] L. Zan, W. Fa, T. Peng, Z.K. Gong, Photocatalysis effect of nanometer TiO2 and TiO2-coated ceramic plate on hepatitis B virus, J. Photochem. Photobiol. B 86 (2007) 165–169, https://doi.org/10.1016/j.jphotobiol.2006.09.002.
[16] R. Matsuura, C.W. Lo, S. Wada, J. Somei, H. Ochiai, T. Murakami, N. Saito, T. Ogawa, A. Shinjo, Y. Benno, M. Nakagawa, M. Takei, Y. Aida, SARS-CoV-2 disinfection of air and surface contamination by TiO2 photocatalyst-mediated damage to viral morphology, RNA, and protein, Viruses 13 (2021) 942–955, https://doi.org/10.3390/v13050942.
[17] P. Micochova, A. Chadha, T. Hesseloj, F. Fraternali, J.J. Ramsden, R.K. Gupta, Rapid inactivation of SARS-CoV-2 by titanium dioxide surface coating, Wellcome Open Res. 6 (2021) 56–68, https://doi.org/10.12688/wellcomeopenres.16577.2.
[18] Y. Tong, G. Shi, G. Hu, X. Hu, L. Han, X. Xie, Y. Xu, R. Zhang, J. Sun, J. Zhong, Photo-catalyzed TiO2 inactivates pathogenic viruses by attacking viral genome, Chem. Eng. J. 414 (2021), 128788, https://doi.org/10.1016/j.cej.2021.128788.
[19] S. Khaiboullina, T. Uppal, N. Dhabarde, V.R. Subramanian, S.C. Verma, Inactivation of human coronavirus by titania nanoparticle coatings and UVC radiation: throwing light on SARS-CoV-2, Viruses 13 (2021) 1–15, https://doi.org/10.3390/v13010019.
[20] M. Gong, S. Xiao, X. Yu, C. Dong, J. Ji, D. Zhang, M. Xing, Research progress of photocatalytic sterilization over semiconductors, RSC Adv. 9 (2019) 19278–19284, https://doi.org/10.1039/C9RA01826C.
[21] A. Mills, C. O'Rourke, K. Moore, Powder semiconductor photocatalysis in aqueous solution: an overview of kinetics-based reaction mechanisms, J. Photochem. Photobiol. A 310 (2015) 66–105, https://doi.org/10.1016/j.jphotochem.2015.04.011.
[22] A. Mills, R. Andrews, R. Han, C. O'Rourke, S. Hodgen, Supersensitive test of photocatalytic activity based on ISO 22197-1:2016 for the removal of NO, J. Photochem. Photobiol. A 400 (2020), 112734, https://doi.org/10.1016/j.jphotochem.2020.112734.
[23] Y. Paz, Z. Luo, L. Rabenberg, A. Heller, Photooxidative self-cleaning transparent titanium dioxide films on glass, J. Mater. Res. 10 (1995) 2842–2848, https://doi.org/10.1557/JMR.1995.2842.
[24] E.A. Kozlova, A.S. Safatov, S.A. Kiselev, V.Yu. Marchenko, A.A. Sergeev, M. O. Skarnovich, E.K. Emelyanova, M.A. Smetannikova, G.A. Buryak, A. V. Vorontsov, Inactivation and mineralization of aerosol deposited model pathogenic microorganisms over TiO2 and Pt:TiO2, Environ. Sci. Technol. 44 (2010) 5121–5126, https://doi.org/10.1021/es100156p.
[25] Y. Chen, D.D. Dionysiou, TiO2 photocatalytic films on stainless steel: the role of Degussa P-25 in modified sol–gel methods, Appl. Catal. B 62 (2006) 255–264, https://doi.org/10.1016/j.apcatb.2005.07.017.
[26] J.A. Byrne, B.R. Eggins, N.M.D. Brown, B. McKinney, M. Rouse, Immobilisation of TiO2 powder for the treatment of polluted water, Appl. Catal. B 17 (1998) 25–36, https://doi.org/10.1016/S0926-3373(97)00101-X.
[27] H. Cui, J. Jiang, W. Gu, C. Sun, D. Wu, T. Yang, G. Yang, Photocatalytic inactivation efficiency of anatase nano-TiO2 sol on the H9N2 avian influenza virus, Photochem. Photobiol. 86 (2010) 1135–1139, https://doi.org/10.1111/j.1751-1097.2010.00763.x.
[28] S.-M. Lam, K.-C. Chew, J.-C. Sin, H. Zeng, H. Lin, H. Li, J.W. Lim, A.R. Mohamed, Ameliorated photodegradation performance of polyethylene and polystyrene films incorporated with ZnO-PVP catalyst, J. Environ. Chem. Eng. 10 (2022), 107594, https://doi.org/10.1016/j.jece.2022.107594.
[29] S.-M. Lam, J.-C. Sin, H. Zeng, H. Lin, H. Li, Y.-Y. Chai, M.-K. Choong, A. R. Mohamed, Green synthesis of Fe-ZnO nanoparticles with improved sunlight photocatalytic performance for polyethylene film deterioration and bacterial inactivation, Mater. Sci. Semicond. Process. 123 (2021), 105574, https://doi.org/10.1016/j.mssp.2020.105574.
[30] S. Fukuyama, H. Katsura, D. Zhao, M. Ozawa, T. Ando, J.E. Shoemaker, I. Ishikawa, S. Yamada, G. Neumann, S. Watanabe, H. Kitano, Y. Kawaoka, Multi-spectral fluorescent reporter influenza viruses (color-flu) as powerful tools for in vivo studies, Nat. Commun. 6 (2015) 6600, https://doi.org/10.1038/ncomms7600.
[31] ViralZone. https://viralzone.expasy.org. Accessed April 2022.
[32] A. Slater, N. Nair, R. Suett, R. Mac Donnchadha, C. Bamford, S. Jasim, D. Livingstone, E. Hutchinson, Visualising viruses, J. Gen. Virol. 103 (2022), 001730, https://doi.org/10.1099/jgv.0.001730.
[33] Wikipedia, Severe Acute Respiratory Syndrome Coronavirus 2. https://en.wikipedia.org/wiki/Severe_acute_respiratory_syndrome_coronavirus_2. Accessed April 2022.
[34] M. Carocci, L. Bakkali-Kassimi, The encephalomyocarditis virus, Virulence 3 (2012) 351–367, https://doi.org/10.4161/viru.20573.
[35] S.J. Rihn, A. Merits, S. Bakshi, M.L. Turnbull, A. Wickenhagen, A.J.T. Alexander, C. Baillie, B. Brennan, F. Brown, K. Brunker, S.R. Bryden, K.A. Burness, S. Carmichael, S.J. Cole, V.M. Cowton, P. Davies, C. Davis, G. De Lorenzo, C. L. Donald, M. Dorward, J.I. Dunlop, M. Elliott, M. Fares, A. da Silva Filipe, J. R. Freitas, W. Furnon, R.J. Gestuveo, A. Geyer, D. Giesel, D.M. Goldfarb, N. Goodman, R. Gunson, C.J. Hastie, V. Herder, J. Hughes, C. Johnson, N. Johnson, A. Kohl, K. Kerr, H. Leech, L.S. Lello, K. Li, G. Lieber, X. Liu, R. Lingala, C. Loney, D. Mair, M.J. McElwee, S. McFarlane, J. Nichols, K. Nomikou, A. Orr, R.J. Orton, M. Palmarini, Y.A. Parr, R.M. Pinto, S. Raggett, E. Reid, D.L. Robertson, J. Royle, N. Cameron-Ruiz, J.G. Shepherd, K. Smollett, D.G. Stewart, M. Stewart, E. Sugrue, A.M. Szemiel, A. Taggart, E.C. Thomson, L. Tong, L.S. Torrie, R. Toth, M. Varjak, S. Wang, S.G. Wilkinson, P.G. Wyatt, E. Zusinaite, D.R. Alessi, A.H. Patel, A. Zaid, S.J. Wilson, S. Mahalingam, A plasmid DNA-launched SARS-CoV-2 reverse genetics system and coronavirus toolkit for COVID-19 research, PLoS Biol. 19 (2021), e3001091, https://doi.org/10.1371/journal.pbio.3001091.
[36] C.G.G. Bamford, L. Broadbent, E. Aranday-Cortes, M. McCabe, J. McKenna, D. G. Courtney, O. Touzelet, A. Ali, G. Roberts, G. Lopez Campos, D. Simpson, C. McCaughey, D. Fairley, K. Mills, U.F. Power, I., On behalf of the breathing together, comparison of SARS-CoV-2 evolution in paediatric primary airway epithelial cell cultures compared with vero-derived cell lines, Viruses 14 (2022) 325–329, https://doi.org/10.3390/v14020325.
[37] M. Ratova, A. Mills, Antibacterial titania-based photocatalytic extruded plastic films, J. Photochem. Photobiol. A 299 (2015) 159–165, https://doi.org/10.1016/j.jphotochem.2014.11.014.
[38] ISO 10678:2010, Fine ceramics (advanced ceramics, advanced technical ceramics) Determination of photocatalytic activity of surfaces in an aqueous medium by degradation of methylene blue, ISO, Geneva, 2010. https://www.iso.org/standard/46019.html. Accessed April 2022.
[39] C.C. van Heerwaarden, W.B. Mol, M.A. Veerman, I. Benedict, B.G. Heusinkveld, W. H. Knap, S. Kazadzis, N. Kouremeti, S. Fiedler, Record high solar irradiance in Western Europe during first COVID-19 lockdown largely due to unusual weather, Commun. Earth Environ. 2 (37) (2021) 1–7, https://doi.org/10.1038/s43247-021-00110-0.
[40] L.J. Reed, H. Muench, A simple method of estimating fifty percent endpoints, Am. J. Epidemiol. 27 (1938) 493–497, https://doi.org/10.1093/oxfordjournals.aje.a118408.
[41] A. Mills, An overview of the methylene blue ISO test for assessing the activities of photocatalytic films, Appl. Catal. B: Environ. 128 (2012) 144–149, https://doi.org/10.1016/j.apcatb.2012.01.019.
[42] J. Tschirch, R. Dillert, D. Bahnemann, B. Proft, A. Biedermann, B. Goer, Photodegradation of methylene blue in water, a standard method to determine the activity of photocatalytic coatings? Res. Chem. Intermed. 34 (2008) 381–392, https://doi.org/10.1163/156856708784040588.
[43] A.A. Selifonov, O.G. Shapoval, A.N. Mikerov, V.V. Tuchin, Determination of the diffusion coefficient of methylene blue solutions in dentin of a human tooth using reflectance spectroscopy and their antibacterial activity during laser exposure, Opt. Spectrosc. 126 (2019) 758–768, https://doi.org/10.1134/S0030400X19060213.
[44] The Electrochemical Society, Electrochemistry Dictionary & Encyclopedia. https://knowledge.electrochem.org/ed/dict.htm#d28. Accessed April 2022.
[45] A. Mills, M. Crow, In situ, continuous monitoring of the photoinduced superhydrophilic effect: influence of UV-type and ambient atmospheric and droplet composition, J. Phys. Chem. C 111 (2007) 6009–6016, https://doi.org/10.1021/jp068327v.
[46] M. Drdacky, J. Lesak, S. Rescic, Z. Slizkova, P. Tiano, J. Valach, Standardization of peeling tests for assessing the cohesion and consolidation characteristics of historic stone surfaces, Mater. Struct. 45 (2012) 505–520, https://doi.org/10.1617/s11527-011-9778-x.
[47] P.D. Rakowska, M. Tiddia, N. Faruqui, C. Bankier, Y. Pei, A.J. Pollard, J. Zhang, I. S. Gilmore, Antiviral surfaces and coatings and their mechanisms of action, Commun. Mater. 2 (53) (2021) 1–19, https://doi.org/10.1038/s43246-021-00153-y.
[48] S. Ye, K. Shao, Z. Li, N. Guo, Y. Zuo, Q. Li, Z. Lu, L. Chen, Q. He, H. Han, Antiviral activity of graphene oxide: how sharp edged structure and charge matter, ACS Appl. Mater. Interfaces 7 (2015) 21571–21579, https://doi.org/10.1021/acsami.5b06876.
[49] S. Pandit, Z. Cao, V.R.S.S. Mokkapati, E. Celauro, A. Yurgens, M. Lovmar, F. Westerlund, J. Sun, I. Mijakovic, Vertically aligned graphene coating is bactericidal and prevents the formation of bacterial biofilms, Adv. Mater. Interfaces 5 (2018) 1701331, https://doi.org/10.1002/admi.201701331.
[50] W. Wei, J. Li, Z. Liu, Y. Deng, D. Chen, P. Gu, G. Wang, X. Fan, Distinct antibacterial activity of a vertically aligned graphene coating against Gram-positive and Gram-negative bacteria, J. Mater. Chem. B 8 (2020) 6069–6079, https://doi.org/10.1039/D0TB00417K.
[51] J. Hasan, Y. Xu, T. Yarlagadda, M. Schuetz, K. Spann, P.K.D.V. Yarlagadda, Antiviral and antibacterial nanostructured surfaces with excellent mechanical properties for hospital applications, ACS Biomater. Sci. Eng. 6 (2020) 3608–3618, https://doi.org/10.1021/acsbiomaterials.0c00348.
[52] M.M. Jensen, Inactivation of airborne viruses by ultraviolet irradiation, Appl. Microbiol. 12 (1964) 418–420, https://doi.org/10.1128/am.12.5.418-420.1964.
[53] C.-C. Tseng, C.-S. Li, Inactivation of viruses on surfaces by ultraviolet germicidal irradiation, J. Occup. Environ. Hyg. 4 (2007) 400–405, https://doi.org/10.1080/15459620701329012.
[54] K.R. Wigginton, B.M. Pecson, T. Sigstam, F. Bosshard, T. Kohn, Virus inactivation mechanisms: impact of disinfectants on virus function and structural integrity, Environ. Sci. Technol. 46 (2012) 12069–12078, https://doi.org/10.1021/es3029473.
[55] Wikipedia, Ultraviolet. https://en.wikipedia.org/wiki/Ultraviolet. Accessed April 2022.
[56] M. Biasin, S. Strizzi, A. Bianco, A. Macchi, O. Utyro, G. Pareschi, A. Loffreda, A. Cavalleri, M. Lualdi, D. Trabattoni, C. Tacchetti, D. Mazza, M. Clerici, UV and

violet light can neutralize SARS-CoV-2 infectivity, J. Photochem. Photobiol. 10 (2022), 100107, https://doi.org/10.1016/j.jpap.2021.100107.
[57] A. Gamble, R.J. Fischer, D.H. Morris, C.K. Yinda, V.J. Munster, J.O. Lloyd-Smith, Heat-treated virus inactivation rate depends strongly on treatment procedure: illustration with SARS-CoV-2, Appl. Environ. Microbiol. 87 (2021) 1–9, https://doi.org/10.1128/AEM.00314-21.
[58] F.E. Buckland, D.A.J. Tyrrell, Loss of infectivity on drying various viruses, Nature 195 (1962) 1063–1064, https://doi.org/10.1038/1951063a0.
[59] C. Batéjat, Q. Grassin, J.-C. Manuguerra, I. Leclercq, Heat inactivation of the severe acute respiratory syndrome coronavirus 2, J. Biosafe. Biosecurity 3 (2021) 1–3, https://doi.org/10.1016/j.jobb.2020.12.001.
[60] M. Liu, K. Sunada, K. Hashimoto, M. Miyauchi, Visible-light sensitive Cu(ii)–TiO2 with sustained anti-viral activity for efficient indoor environmental remediation, J. Mater. Chem. A 3 (2015) 17312–17319, https://doi.org/10.1039/C5TA03756E.
[61] R. Nakano, M. Hara, H. Ishiguro, Y. Yao, T. Ochiai, K. Nakata, T. Murakami, J. Kajioka, K. Sunada, K. Hashimoto, A. Fujishima, Y. Kubota, Broad spectrum microbicidal activity of photocatalysis by TiO2, Catalysts 3 (2013) 310–323, https://doi.org/10.3390/catal3010310.
[62] X. Sang, T.G. Phan, S. Sugihara, F. Yagyu, S. Okitsu, N. Maneekarn, W.E. Muller, H. Ushijima, Photocatalytic inactivation of diarrheal viruses by visible-light-catalytic titanium dioxide, Clin. Lab. 53 (2007) 413–421. https://pubmed.ncbi.nlm.nih.gov/17821945/.
[63] P.N.M. Shah, D.J. Filman, K.S. Karunatilaka, E.L. Hesketh, E. Groppelli, M. Strauss, J.M. Hogle, Cryo-EM structures reveal two distinct conformational states in a picornavirus cell entry intermediate, PLoS Pathog. 16 (2020), e1008920, https://doi.org/10.1371/journal.ppat.1008920.
[64] M. Hauser, W.J. Dearnaley, A.C. Varano, M. Casasanta, S.M. McDonald, D.F. Kelly, Cryo-EM reveals architectural diversity in active rotavirus particles, Comput. Struct. Biotechnol. J. 17 (2019) 1178–1183, https://doi.org/10.1016/j.csbj.2019.07.019.